SUPPORTING INFORMATION

Influence of conformation on conductance of biphenyl-dithiol single-molecule contacts

Artem Mishchenko[1], David Vonlanthen[2], Velimir Meded[3], Marius Bürkle[4], Chen Li[1], Ilya V. Pobelov[1], Alexei Bagrets[3], Janne K. Viljas[4], Fabian Pauly[4], Ferdinand Evers[3,5], Marcel Mayor[2,3], and Thomas Wandlowski[1]

[1]*Department of Chemistry and Biochemistry, University of Bern, 3012 Bern, Switzerland*

[2]*Department of Chemistry, University of Basel, 4003 Basel, Switzerland*

[3]*Institute of Nanotechnology, Research Center Karlsruhe, P.O. Box 3640, 76021 Karlsruhe, Germany*

[4]*Institut für Theoretische Festkörperphysik, University of Karlsruhe, 76128 Karlsruhe, Germany*

[5]*Institut für Theorie der Kondensierten Materie, University of Karlsruhe, 76128 Karlsruhe, Germany*

I. EXPERIMENTAL PROCEDURES

A. Single-molecule-conductance measurement

The conductance of single-molecule junctions was studied using an STM-break-junction (STM-BJ) approach for measuring the current through a molecule trapped between the tip of an STM and the sample electrode. In this section we provide an extended description of the measurement procedure, which was partially described in our previous publications.[1]

The sample electrodes were Au(111) disks of 2 mm height and 10 mm in diameter. The Au(111) substrates were flame-annealed prior to use. A freshly prepared 250 μM solution of the respective molecule dissolved in a 4:1 mixture of 1,3,5-trimethylbenzene (mesitylene) and tetrahydrofurane was added to a liquid cell (Kel-F) mounted on top of the sample electrode. Deprotection of the thiol groups was achieved by adding tetrabutylammonium hydroxide up to the final concentration of 125 μM. The gold STM tips were prepared by electrochemical etching of gold wires (99.999%, 0.25 mm diameter) in a 1:1 mixture of 30% HCl and ethanol.[2]

All experiments were carried out at room temperature using a modified Molecular Imaging PicoSPM. The PicoSPM head was placed in a custom-made, gas-tight glass chamber filled with high-purity Ar (CarbaGas, 99.999%) to prevent oxygen exposure and contamination from air. The standard STM scanner was replaced by a STM scanner with a modified dual channel preamplifier.[3] The input current was simultaneously converted to two voltage signals (range $\pm$10 V) with the conversion factors 21 μA/V (high range) and 10 nA/V (low range). Both signals were split, and the original as well as the 10 times amplified signals were recorded. The current was measured in an extraordinary wide range of 1 pA to 150 μA with high resolution. The non-amplified low-range current signal was fed back to the STM controller, preserving the original STM imaging capability of the PicoSPM.

The current-distance measurements were performed with a separate, lab-built analog ramp unit (PC + National Instruments PCI-6040E I/O Card + analog ramp circuit + self-written software). It was connected to the lab-made break box, wired between the STM controller and the measuring head. This arrangement enabled the controlling software to read out current signals as well as to control the vertical position of the tip by feeding the voltage to the piezo element driving the vertical tip movement. Finally, four current signals were

directed from a break box to a digital oscilloscope Yokogawa DL750 for simultaneous data recording with 16bit resolution and a sampling rate of 1 MS·sec^{-1}.

The STM-BJ experiments were carried out according to the following procedure. After approach of the STM tip to the Au(111) surface a few images were recorded in order to inspect the sample and to select a defect-free area for further measurements. The tip was then brought to an appropriate lateral position and stabilized by the STM feedback at a fixed tip-sample separation corresponding to the preset value of the tunneling current (typically 0.1 nA). Current-distance measurements were then performed at a fixed lateral position with the STM feedback switched off and the vertical tip movement controlled by the ramp unit described above. The measuring cycle was performed in the following way. First, the controlling software drives the STM tip towards the surface. Simultaneously the current through the junction is monitored. The approach was stopped when a pre-defined upper current limit was reached. Under the present experimental condition with molecule-containing solutions the latter was typically 50 μA. After a short ($\approx$100 ms) delay, ensuring tip relaxation and formation of stable contacts, the tip was withdrawn by 2 to 5 nm until the low current limit of $\approx$10 pA is reached. The approaching and withdrawal of the tip were performed with a rate of about 60 nm·s^{-1}. The current-time traces were recorded during the withdrawing step with a digital oscilloscope triggered by the drop of current below 20 μA. The above cycle was repeated in several series of $\approx$3000 traces at each set of experimental conditions to ensure the statistical significance of the results. For each molecule the data were recorded at three different bias voltages of 0.065, 0.1 and 0.18 V.

B. Data analysis

The raw data, as saved with a digital oscilloscope in binary format, were analyzed with a lab-made software implemented in LabView 8.6. The data analysis method was similar to the one proposed in ref 4. Plateaus between abrupt changes in conductance traces were collected to build the conductance histograms. The following procedure was applied: Firstly, for each conductance trace a *Median Filter* was applied to smooth the plateau region but not the abrupt steps. Secondly, the negative of the first derivative was computed and a *Savitzky-Golay Filter* was chosen to smooth it. Only peaks higher than a certain threshold (0.002-0.005 in units of the derivative) were considered further. The distance between two

successive peaks (i.e. the plateau length) was calculated and only plateaus longer than 0.05 nm were processed further. The mean value, the standard deviation, and the slope (obtained from a linear fit of the plateau region) were used for further selection of plateaus. Finally, if a plateau was selected, the untreated data points of the plateau region were used to build the conductance histogram. All such conductance histograms were summed up. After processing all the data, peaks on conductance histograms were fitted with a log-normal distribution

$$f(x;\mu,\sigma,A,y_0) = y_0 + \frac{A}{x\sigma\sqrt{2\pi}} \cdot \exp\left(-\frac{[\ln(x)-\mu]^2}{2\sigma^2}\right), \tag{1}$$

where μ and σ are the mean and the standard deviation of $\ln(x)$, A is the area under the curve, and y_0 is a small offset value. The peak position of $\exp(\mu - \sigma^2)$ was taken as the most probable conductance value. The length of the selected plateaus was used to construct plateau length histograms.

C. Conductance histograms

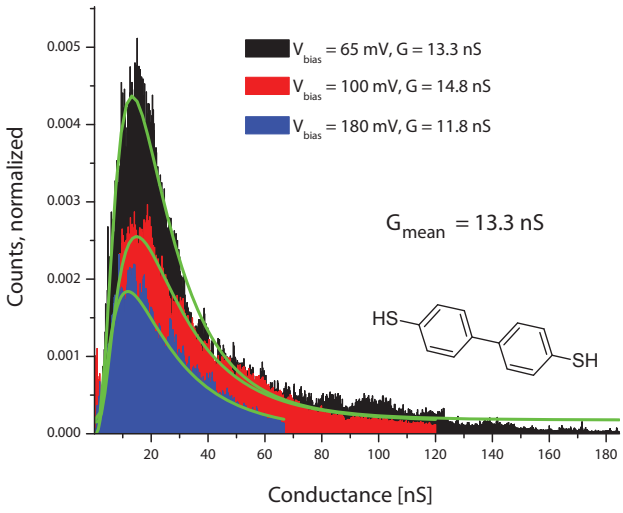

FIG. S1: Plateau-point histograms for **M1**: (black) $V_{\text{bias}} = 0.065$ V, (red) $V_{\text{bias}} = 0.1$ V, (blue) $V_{\text{bias}} = 0.18$ V. The average conductance value, G_{mean}, was obtained from measurements with different bias voltages.

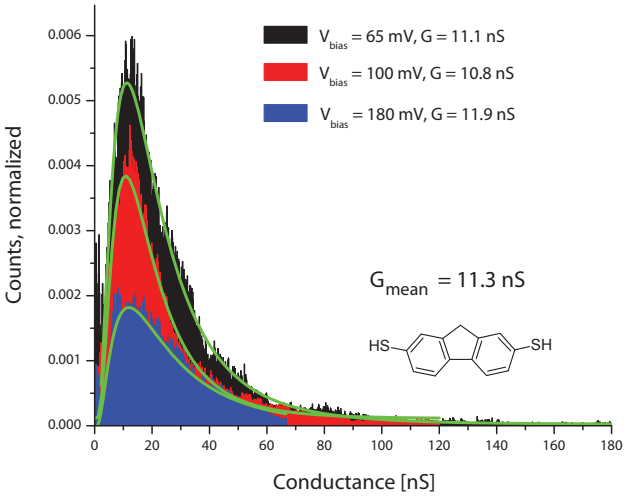

FIG. S2: Plateau-point histograms for **M2**: (black) $V_{\text{bias}} = 0.065$ V, (red) $V_{\text{bias}} = 0.1$ V, (blue) $V_{\text{bias}} = 0.18$ V.

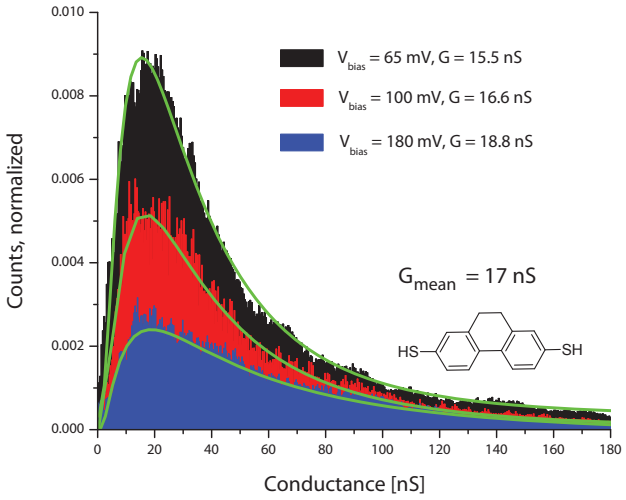

FIG. S3: Plateau-point histograms for **M3**: (black) $V_{\text{bias}} = 0.065$ V, (red) $V_{\text{bias}} = 0.1$ V, (blue) $V_{\text{bias}} = 0.18$ V.

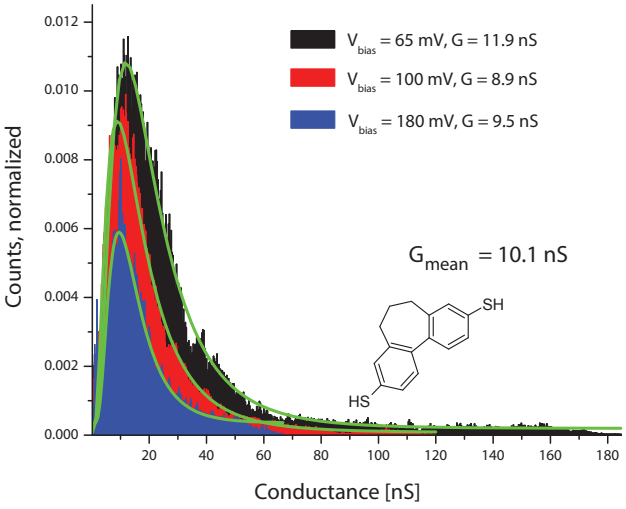

FIG. S4: Plateau-point histograms for **M4**: (black) $V_{\text{bias}} = 0.065$ V, (red) $V_{\text{bias}} = 0.1$ V, (blue) $V_{\text{bias}} = 0.18$ V.

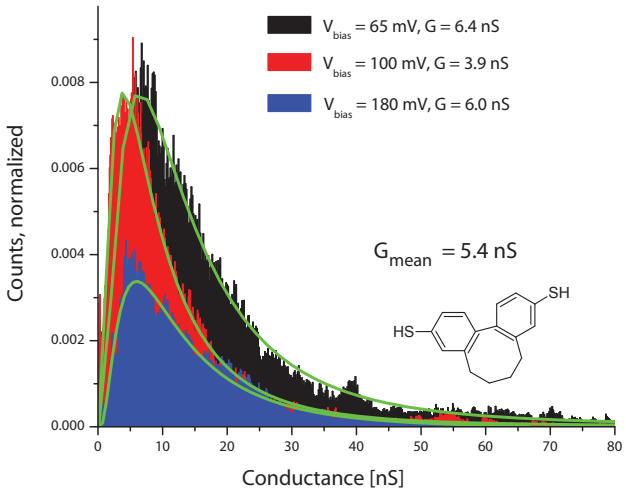

FIG. S5: Plateau-point histograms for **M5**: (black) $V_{\text{bias}} = 0.065$ V, (red) $V_{\text{bias}} = 0.1$ V, (blue) $V_{\text{bias}} = 0.18$ V.

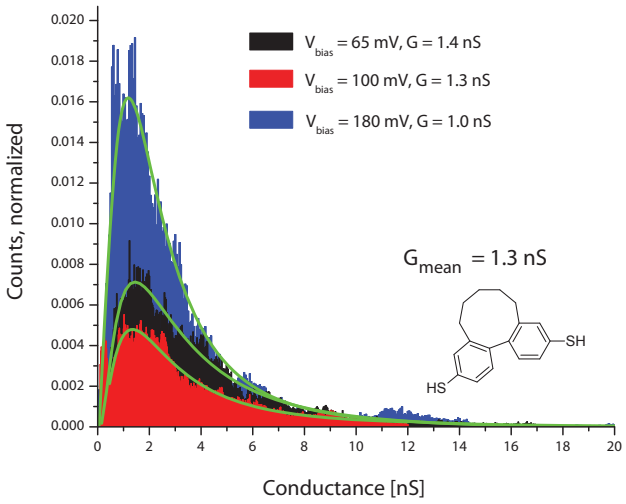

FIG. S6: Plateau-point histograms for **M6**: (black) $V_{\text{bias}} = 0.065$ V, (red) $V_{\text{bias}} = 0.1$ V, (blue) $V_{\text{bias}} = 0.18$ V.

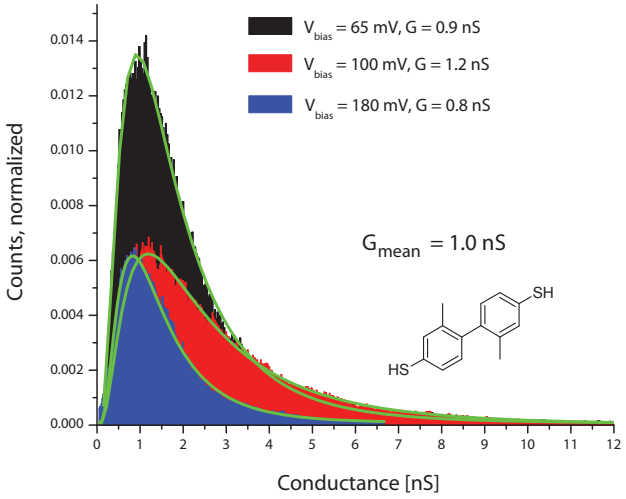

FIG. S7: Plateau-point histograms for **M7**: (black) $V_{\text{bias}} = 0.065$ V, (red) $V_{\text{bias}} = 0.1$ V, (blue) $V_{\text{bias}} = 0.18$ V.

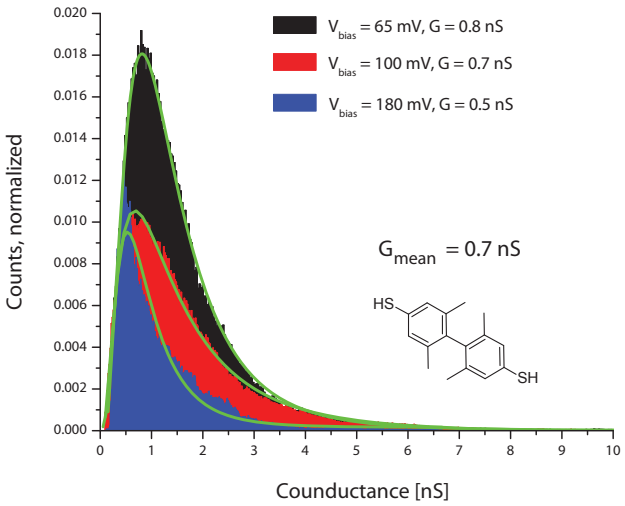

FIG. S8: Plateau-point histograms for **M8**: (black) $V_{\text{bias}} = 0.065$ V, (red) $V_{\text{bias}} = 0.1$ V, (blue) $V_{\text{bias}} = 0.18$ V.

II. THEORETICAL PROCEDURES

D. Molecular structure and contact geometries

In order to explore possible geometries of the molecules in the junctions, in particular with respect to their conformation, we start with an analysis of the isolated biphenyl derivatives **M1**–**M8**. For them, our calculations based on density functional theory (DFT) indicate that the torsion angle φ depends only slightly on the termination, such as H, S-H, or S-Au_1 (see Table S1). Exceptions are **M1** and **M6**. We find at least two different minimum-energy structures for **M6** due to different configurations of the rather long alkyl chains. The value of φ, given in the table, corresponds to the one with the lowest energy.

In these calculations, we find it necessary to work with very strict convergence criteria for the structure relaxation; we let the norm of the Cartesian decay to values below 10^{-5} a.u. Moreover, we mention that the individual two benzene rings have slight deviations from a planar structure. As a consequence, the definition of *the* torsion angle is unique to within 1°.

For the junctions, we have analyzed two different bonding coordinations. In the atop-atop coordination the sulfur is bonded to a single gold atom of each electrode, while these are

TABLE S1: Torsion angles φ between adjacent phenyl rings as calculated for molecules **M1**–**M8** with different terminal groups and for the two different bonding positions in gold junctions.

	Terminal group / bonding position				
Molecule	H φ (deg)	S-H φ (deg)	S-Au_1 φ (deg)	top-top φ (deg)	bridge-bridge φ (deg)
M1	36.4	44.9	34.2	34.2	12.9
M2	0.0	2.4	2.0	2.0	0.1
M3	20.4	20.3	18.9	18.9	19.3
M4	47.5	46.7	46.4	46.4	42.1
M5	61.7	61.3	61.1	61.1	53.0
M6	89.0	70.5	72.0	72.0	62.5
M7	87.5	89.7	86.9	86.9	50
M8	90.0	89.6	88.6	88.6	84.0

two on each side for bridge-bridge coordination. To determine realistic junction structures, we have adopted different procedures for optimizing the geometries as described below. The values of φ obtained under the various conditions are summarized in Table S1. Deviations in torsion angles between atop-atop and bridge-bridge bonding indicate a low stability of the molecular conformations.

For the atop-atop bonding geometry, the optimized molecular structures with S-Au_1 termination are used [see Figure S9(A)]. Thereafter, two electrodes, with their lattice constant set to the experimental value of 0.408 nm and represented by finite-size gold clusters, are attached to both ends. Their orientation is chosen in such a way that the S-Au_1 axis coincides with the [100] direction of the pyramid-shaped Au clusters [see Figure S9(B)]. As a consequence, atomic layers of the left and right electrodes are in general misaligned. By construction the torsion angle φ agrees with those of the isolated, S-Au_1-terminated molecule.

Instead, for bridge-bridge bonding, atomic layers of the left and right [111] electrodes are kept parallel to each other. As a first step, the geometric structure of an S-Au_1-terminated molecule is computed, bonded to a single Au pyramid in the bridge position [see Figure S9(C)]. As indicated to the right, the two atomic layers closest to the molecule are included in the optimization. Next, a second pyramid is attached, and we impose the Bravais lattices

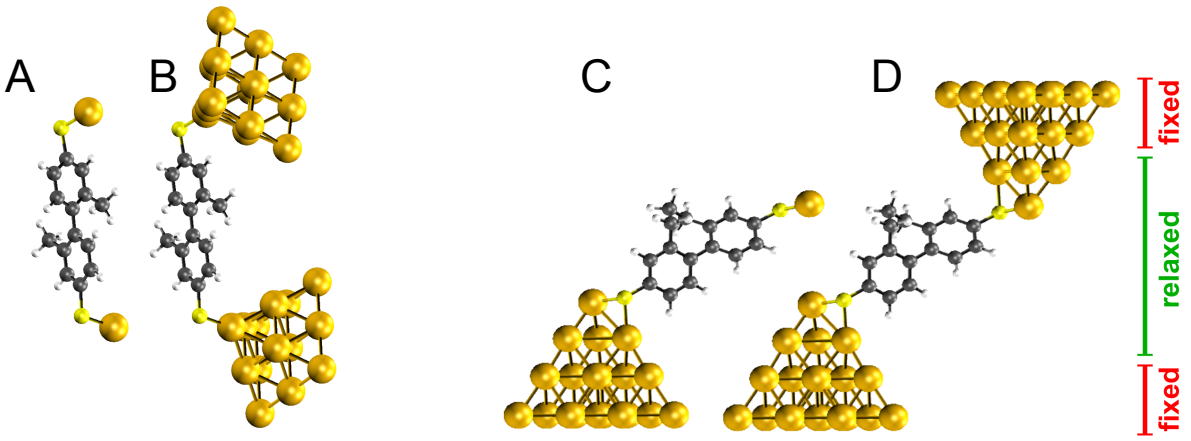

FIG. S9: Steps involved in the determination of contact geometries: (A,B) atop-atop and (C,D) bridge-bridge coordination.

of the two electrodes to be oriented in the same way. The atomic positions of the molecule and of the two atomic layers closest to the molecule are again optimized [see Figure S9(D)]. In this way, the molecule adjusts itself to the constraint imposed by the contacts, and torsion angles may differ from those of the S-Au_1-terminated molecule.

Due to the parallel atomic layers, the electrodes in the bridge-bridge junctions can be thought of as originating from the rupture of a large single crystal. In the atop-atop geometry, instead, the electrodes are assumed to exhibit a certain flexibility to adjust to the molecular geometry. The procedures for structure optimization can be thought of as two limiting cases of the experimental situation. While the gold electrodes certainly put a geometric constraint on the molecule, at the room temperature both the molecule and the metal will be rather flexible.

E. Two-level model

The two-level model (TLM), eq (1), describes the transport through the HOMO resonances of the biphenyl-dithiol derivatives. In the off-resonant situation relevant for the experiments, it factorizes into the two components T_Γ and T_{V1}, as explained in the main text. They can be interpreted as transmission through a single benzene ring and from ring to ring, respectively.

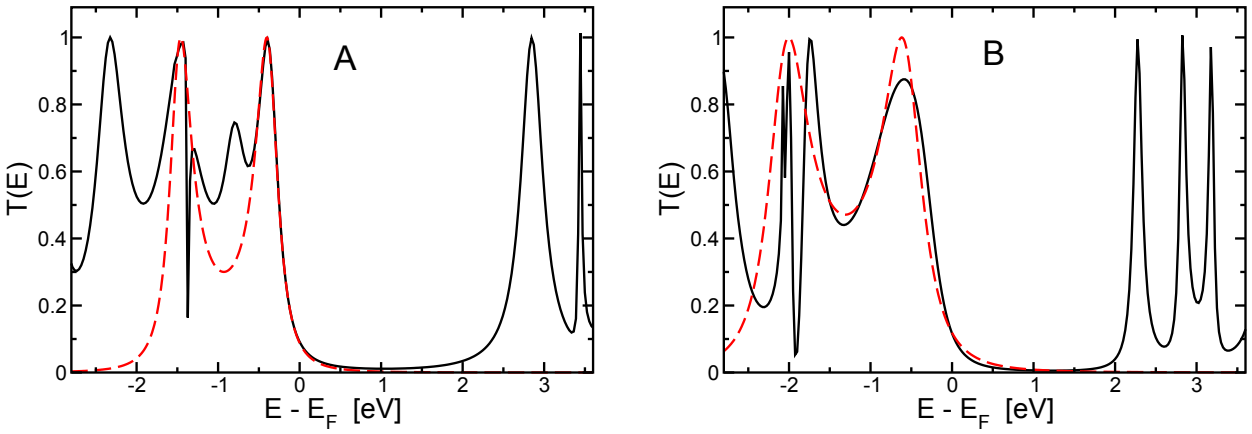

FIG. S10: Transmission $T(E)$ through **M3** as obtained from DFT-based calculations. Dashed lines are fits using the TLM, eq (1): (A) atop-atop, data fit with $\epsilon_0 - E_F = -0.93$ eV, $V_1 = 0.59$ eV, and $\Gamma = 0.33$ eV and (B) bridge-bridge coordination, data fit with $\epsilon_0 - E_F = -1.31$ eV, $V_1 = 0.8$ eV, and $\Gamma = 0.6$ eV.

To obtain estimates for the three parameters ϵ_0, V_1, and Γ of the TLM, we fitted eq (1) to the transmissions $T(E)$ as determined from DFT. An example is shown in Figure S10 for **M3** in the two different bonding coordinations, atop-atop and bridge-bridge.

Special emphasis in the fit has been put on the reproduction of the transmission at the Fermi energy E_F as well as the position of the doublet, $\epsilon_{a,s}$. The peak at lower energies, ϵ_s, is often obscured due to hybridization of the molecular state with those of sulfur and gold. As is visible from the figure, the full DFT calculation exhibits many more than just two levels. Hence, the parametrization of the TLM model in terms of ϵ_0, V_1, and Γ, is somewhat phenomenological and the corresponding numerical estimates are reasonable but not precise.

Using the parameters ϵ_0, V_1, and Γ extracted from the TLM, the conductance G as a function of φ shows a discernable curvature. This is due to ϵ_a approaching E_F closely. Surprisingly, the dependence $G(\varphi)$ is nevertheless roughly linear in $\cos^2\varphi$ for the DFT data. We attribute this mostly to the decrease of ε_0 for more planar molecules, as visible in Figure 5 and discussed in the text. Due to inaccuracies of DFT with regard to level broadenings and level alignments, we speculate that transport in the experiment could indeed be more strongly off-resonant than predicted by DFT. This provides a second possible explanation – in addition to the nonlinear level flow observed in the DFT calculations – for why the linear relation, $G \propto \cos^2\varphi$, is observed experimentally (see Figure 3) in such a large range

of torsion angles.

---

[1] Li C., Pobelov I., Wandlowski Th., Bagrets A., Arnold A., Evers F., *J. Am. Chem. Soc.*, **2008**, 130, 318.

[2] Ren B., Picardi G., Pettinger B., *Rev. Sci. Instrum.*, **2004**, 75, 837.

[3] Mészáros G., Li C., Pobelov I., Wandlowski Th. *Nanotechnology*, **2007**, 18, 424004.

[4] Park Y., Whalley A., Kamenetska M., Steigerwald M., Hybertsen M., Nuckolls C., Venkataraman L. *J. Am. Chem. Soc.*, **2007**, 129, 15768.